Computer Physics Communications 181 (2010) 1862–1867

Contents lists available at ScienceDirect

Computer Physics Communications

www.elsevier.com/locate/cpc

Electronic structure packages: Two implementations of the projector augmented wave (PAW) formalism

Marc Torrent [a], N.A.W. Holzwarth [b,*], François Jollet [a], David Harris [b], Nicholas Lepley [b], Xiao Xu [b]

[a] CEA, DAM, DIF, F-91297 Arpajon, France
[b] Department of Physics, Wake Forest University, Winston-Salem, NC 27109, USA

ARTICLE INFO

Article history:
Received 12 May 2010
Received in revised form 9 July 2010
Accepted 23 July 2010
Available online 29 July 2010

Keywords:
Projector Augmented Wave (PAW)
Electronic structure codes

ABSTRACT

The projector augmented wave (PAW) formalism developed by Blöchl [Phys. Rev. B 50 (1994) 17953] is an accurate and efficient pseudopotential-like scheme for electronic structure calculations within density functional theory and is now implemented in several electronic structure codes. Some of these codes use an implementation of the formalism developed by Kresse et al. [Phys. Rev. B 59 (1999) 1758] which differs slightly from the original Blöchl formalism and which can lead to different electronic structure results. In this paper, we analyze and illustrate the difference between the Blöchl and Kresse PAW formulations.

1. Introduction

The tools available for detailed first-principles studies of materials have benefited enormously from the development of several international collaborations engaged in developing open source electronic structure code packages. For example, the WIEN2k [1] package is based on linearized augmented plane wave (LAPW) method [2], while ABINIT [3] and PWSCF [4] are based on several different pseudopotential methods. These collaborations have resulted in well-designed shared codes which incorporate many of the best "state of the art" methodologies. Validation is an important aspect of code development and most of the collaboration teams have incorporated internal tests as part of their development procedures. The availability of several independently developed codes, provides the opportunity for further testing and validation.

The present paper deals with the identification and analysis of a particular discrepancy between two independent codes in their implementation the projector augmented wave (PAW) method developed by Blöchl [5]. The PAW method has been demonstrated to be a particularly efficient and accurate tool for electronic structure calculations, combining the numerical advantages of pseudopotential techniques while retaining the physics of all-electron methods, including representing the correct nodal behavior of the valence-electron wave functions and the inclusion of upper core states in addition to valence states in the self-consistent iterations. We show that the discrepancy can be traced to a slight formalism difference in the two implementations. Since one of the codes (ABINIT) is widely used and because our analysis may be relevant to some of the other codes which have adopted the PAW method, we thought it useful to publish our findings.

Table 1
PAW parameters used in calculations: the pseudopotential radius r_c^a (in bohr), list of shell designations $n_1 l_1(r_{m_1}) n_2 l_2(r_{m_2}) \ldots$ of basis and projector functions used in the calculation and corresponding radii r_{m_i} (in bohr) used to match the all-electron and pseudo radial wavefunctions. The symbol ϵ indicates the use of unbound basis functions with energies $\epsilon = 2.0, 0.0$, and 3.0 Ry for F, Si, and Cu, respectively.

Atom	r_c^a	$\{n_i l_i(r_{m_i})\}$
Li	1.7	1*s*(1.4) 2*s*(1.7) 2*p*(1.7)
F	1.5	2*s*(1.5) ϵ*s*(1.5) 2*p*(1.5) ϵ*p*(1.5)
Si (valence)	2.0	3*s*(2.0) 3*p*(2.0) ϵ*d*(2.0)
Si (semicore)	1.5	2*s*(1.5) 3*s*(1.5) 2*p*(1.5) 3*p*(1.5)
Cu	2.3	3*s*(1.5) 4*s*(2.2) 3*p*(1.5) 4*p*(2.2) 3*d*(1.5) ϵ*d*(2.2)

All calculations were performed within the framework of density functional theory [6,7] using exchange correlation functionals with either the local density approximation (LDA) [8], or the generalized gradient approximation (GGA) [9]. The independent codes used for the comparison of PAW implementations are PWPAW [10] and ABINIT [3] using the same PAW basis and projector functions generated using the ATOMPAW code [11] and the *atompaw2abinit* converter program available at the ABINIT website. These codes have been compared with each other and with other independent codes, and for most materials the agreement is excellent. However, three example materials serve to illustrate the discrepancy. These materials use the PAW basis and projector function parameters listed in Table 1.

The first example is the highly ionic material LiF in the rock-salt structure. Fig. 1 shows plots of electronic energy versus cubic lattice parameter *a*, comparing the PAW results from both PAW codes

* Corresponding author.
E-mail address: natalie@wfu.edu (N.A.W. Holzwarth).

0010-4655/$ – see front matter
doi:10.1016/j.cpc.2010.07.036

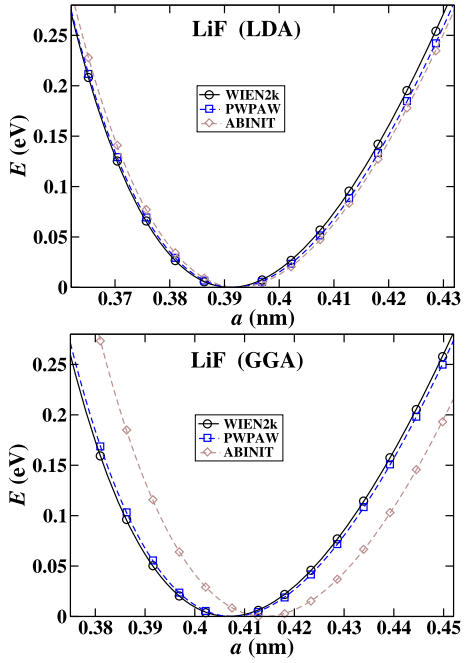

Fig. 1. Plots of electronic energy (E) of LiF as a function of lattice constant (a) determined from the WIEN2k [1], PWPAW [10], and ABINIT [3] codes, comparing LDA [8] (upper plot) and GGA [9] (lower plot) results.

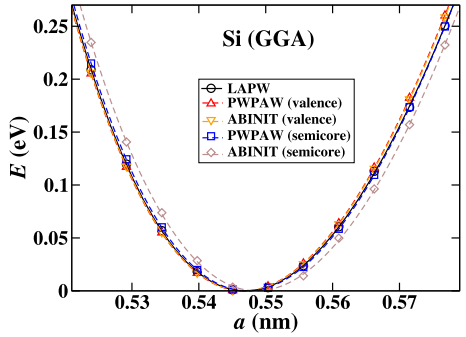

Fig. 2. Plot of the electronic energy (E) of Si as a function of lattice constant (a) calculated using the GGA functional, comparing results using 3 codes and 2 different PAW basis and projector sets as explained in Table 1 and in the text.

with the all-electron results generated by the WIEN2k code. In general there is excellent agreement among all of the results, with the obvious exception of the ABINIT results for the GGA functional, where the equilibrium lattice constant is found to be 0.006 nm larger than that of the others.

The second example is Si in the diamond structure is shown in Fig. 2. In this case, only the GGA results are presented for two different basis and projector sets – "valence" and "semicore" defined in Table 1. We see that while the "valence" basis set gives results in good agreement between WIEN2k, PWPAW, and ABINIT, the "semicore" basis set used with the ABINIT code results in a discrepancy compared the other results. While this discrepancy is not as large as the discrepancy for the GGA functional results of LiF, it is larger than it should be if the codes were performing the same calculations with the same input parameters, as designed.

Finally, in Fig. 3 we show binding energy curves for Cu in the fcc structure, comparing LDA and GGA results. In this case, the PAW calculations used basis and projector functions including semicore states in order to accurately represent the 3d contributions. The results show that there is a small discrepancy between the calculations using the LDA functional and a much larger discrepancy for ABINIT code results using the GGA functional.

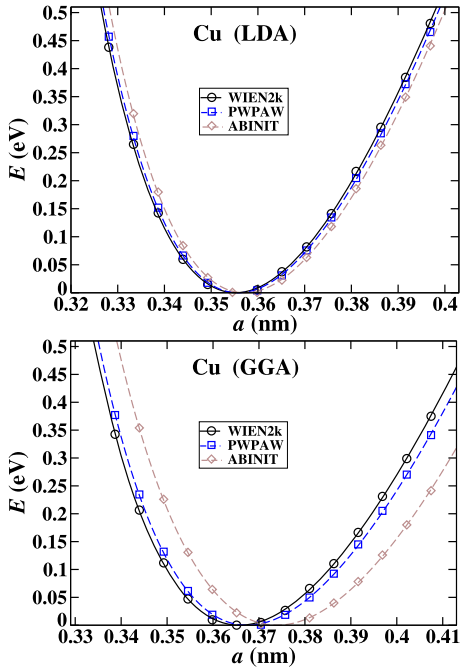

Fig. 3. Plots of electronic energy (E) of Cu as a function of lattice constant (a) comparing results obtained the LDA and GGA functionals and 3 computer codes.

These three examples show extreme examples of the discrepancies between the two codes. By contrast, there are many other materials which show excellent agreement between the two codes. As we will show, the origin of the discrepancies turns out to be due to a subtle difference in formalisms.

In Section 2 we discuss the PAW implementations used by the two codes and identify the terms which cause the discrepancies. In Section 3 we illustrate the behaviors of the problematic terms. Section 4 summarizes the results and discusses several approaches to avoiding this difficulty.

2. Formalism

In addition to the original paper by Blöchl [5], there are now several paper which detail the PAW formalism [10–17]. The basic idea can be summarized in terms of the PAW expression of the valence electron energy of the system as a combination of smooth contributions evaluated over all space plus a sum of atom-centered terms which contribute within "augmentation" spheres, of radii r_c^a about each atomic site a:

$$E_{\text{vale}} = \underbrace{\widetilde{E}_{\text{vale}}}_{\text{pseudo-energy}} + \sum_a \underbrace{\left(E^a_{\text{vale}} - \widetilde{E}^a_{\text{vale}}\right)}_{\text{atom-centered corrections}} . \tag{1}$$

In principle, the pseudo-energy contributions within each augmentation sphere are canceled out of the expression by the atom-centered pseudo-energy $\widetilde{E}^a_{\text{vale}}$ and replaced by the atom-centered full nodal valence energy E^a_{vale}. Provided that the cancellation is well approximated, there is considerable freedom in the formulation of pseudofunctions within the augmentation spheres. Consequently, there are some variations in the detailed formulations of the PAW method described in the literature. The ABINIT formulation [17] follows that of Kresse [14] which, apart from regrouping of the terms in the expressions, differs from the original formulation of Blöchl [5,15] in the treatment of the pseudo exchange–correlation contributions. In particular, denoting by $n(\mathbf{r})$ and $n_c(\mathbf{r})$ the valence and core electron fully nodal charge densities and by $\tilde{n}(\mathbf{r})$ and $\tilde{n}_c(\mathbf{r})$ the corresponding valence and core electron pseu-

dodensities, Blöchl's form of the exchange–correlation energies can be expressed in terms of the functional dependencies:

$$E_{xc}^{\mathrm{B}} = E_{xc}[\tilde{n}+\tilde{n}_c] + \sum_a \left(E_{xc}^a\left[n^a+n_c^a\right] - E_{xc}^a\left[\tilde{n}^a+\tilde{n}_c^a\right]\right). \tag{2}$$

Including the smooth core pseudodensities in the evaluation of the functional follows the notion of the non-linear core correction introduced by Louie et al. [18] which has been demonstrated to work well for norm-conserving pseudopotentials and also works well for the PAW formalism. On the other hand Kresse's version of the exchange–correlation energies has the form

$$E_{xc}^{\mathrm{K}} = E_{xc}[\tilde{n}+\tilde{n}_c+\hat{n}] + \sum_a \left(E_{xc}^a\left[n^a+n_c^a\right] - E_{xc}^a\left[\tilde{n}^a+\tilde{n}_c^a+\hat{n}^a\right]\right). \tag{3}$$

Here the extra term $\hat{n}(\mathbf{r})$ is the valence compensation charge density, which can be defined[1] in the notation of Refs. [14] and [17] to be

$$\hat{n}(\mathbf{r}) = \sum_{aijLM} \rho_{ij}^a \hat{Q}_{ij}^{aLM}(\mathbf{r}), \tag{4}$$

where a is the atomic site index, ij are basis and projector function indices and LM are spherical harmonic indices. The coefficients ρ_{ij}^a are determined from the Bloch pseudowavefunctions $\widetilde{\Psi}_{n\mathbf{k}}(\mathbf{r})$ and the projector functions $\tilde{p}_i^a(\mathbf{r})$ by the expression

$$\rho_{ij}^a = \sum_{n\mathbf{k}} f_{n\mathbf{k}} \langle \widetilde{\Psi}_{n\mathbf{k}} | \tilde{p}_i^a \rangle \langle \tilde{p}_j^a | \widetilde{\Psi}_{n\mathbf{k}} \rangle, \tag{5}$$

where $f_{n\mathbf{k}}$ represents the sampling weight and occupancy of the Bloch state. The compensation spatial functions $\hat{Q}_{ij}^{aLM}(\mathbf{r})$ are localized within the augmentation sphere of atom a and have the form

$$\hat{Q}_{ij}^{aLM}(\mathbf{r}) \equiv q_{ij}^{LM} g_L\left(|\mathbf{r}-\mathbf{R}^a|\right) Y_{LM}\left(\widehat{\mathbf{r}-\mathbf{R}^a}\right), \tag{6}$$

where $Y_{LM}(\widehat{\mathbf{r}-\mathbf{R}^a})$ denotes a spherical harmonic function, q_{ij}^{LM} is a coefficient representing the LMth moment associated with the pair of basis functions i and j, and $g_L(|\mathbf{r}-\mathbf{R}^a|)$ denotes a radial shape function with the properties

$$g_L(r) \equiv 0 \quad \text{for } r \geqslant r_c^a \quad \text{and} \quad \int_0^{r_c^a} dr\, r^{2+L} g_L(r) = 1. \tag{7}$$

The purpose of the compensation charge density $\hat{n}(\mathbf{r})$ is to add the correct amount of charge moments to the valence pseudodensity

$$\tilde{n}(\mathbf{r}) \equiv \sum_{n\mathbf{k}} f_{n\mathbf{k}} \left|\widetilde{\Psi}_{n\mathbf{k}}(\mathbf{r})\right|^2 \tag{8}$$

so that outside the augmentation region of all the atoms, the Coulomb (or Hartree) potential for the sum of the valence pseudo and compensation charge densities $\tilde{n}(\mathbf{r})+\hat{n}(\mathbf{r})$ is the same as that for the fully nodal valence electron density $n(\mathbf{r})$:

$$V_H(\mathbf{r}) = \int d^3r' \frac{\tilde{n}(\mathbf{r}')+\hat{n}(\mathbf{r}')}{|\mathbf{r}-\mathbf{r}'|} \overset{|\mathbf{r}-\mathbf{R}^a|>r_c^a}{=} \int d^3r' \frac{n(\mathbf{r}')}{|\mathbf{r}-\mathbf{r}'|}. \tag{9}$$

While the inclusion of compensation charge density $\hat{n}(\mathbf{r})$ is essential to correctly representing the Coulombic interactions of the system, it is not obvious that $\hat{n}(\mathbf{r})$ has any physical meaning in the argument of exchange–correlation functionals which are based on either a local density approximation (LDA) [8] or a generalized gradient approximation (GGA) [9]. For these functionals, at any given spatial point $\mathbf{r}$, the exchange–correlation contribution depends on the density (and its gradient in the case of GGA) at that point. Formally, all pseudofunction contributions within the augmentation sphere, cancel out of the energy and Hamiltonian expressions, so that in general, the presence of the compensation charge in the exchange–correlation functional the expression should do no harm. However, in some cases, such as those presented in the introduction, inclusion of $\hat{n}(\mathbf{r})$ in the argument of the pseudo exchange–correlation functional can introduce non-canceling errors as will be demonstrated in more detail in Section 3.

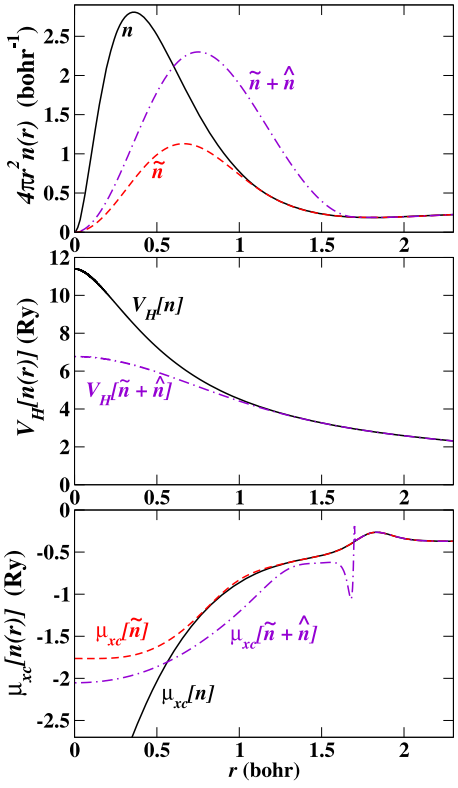

Fig. 4. Plots of radial charge densities (top panel), Hartree potentials (second panel), and GGA exchange–correlation potentials (lower panel) for Li with $r_c^a = 1.7$ bohr. The compensation charge density $\hat{n}$ is constructed using the squared sinc function defined in Eq. (10).

3. Examples

In order to visualize the effects of the two formulations of PAW exchange–correlation contributions, we first consider the example of Li with the GGA functional and the PAW parameters listed in Table 1. In order to describe correct behavior in the highly ionic compound of LiF, all 3 electrons of Li are treated as valence electrons ($n_c \equiv 0$ and $\tilde{n}_c \equiv 0$). Fig. 4 shows plots of the all-electron density $n(r)$, the pseudodensity $\tilde{n}(r)$, and the sum of the pseudodensity and the compensation charge density $\tilde{n}(r)+\hat{n}(r)$. In these calculations, the squared sinc function was used for the compensation charge shape:

$$g_L(r) = \begin{cases} \mathcal{N}_L r^L \left(\frac{\sin(\pi r/r_c^a)}{\pi r/r_c^a}\right)^2 & \text{for } r \leqslant r_c^a, \\ 0 & \text{for } r > r_c^a, \end{cases} \tag{10}$$

where $\mathcal{N}_L$ is a normalization constant. The middle panel of Fig. 4 shows the Hartree potentials which results from these charges. The Hartree potential for the sum of the pseudodensity and the compensation charge density smoothly converges to the correct

[1] In Ref. [5] and several others, the definition of the compensation charge density $\hat{n}(\mathbf{r})$ includes nuclear and core electron contributions which are NOT included in the present formulation, but are treated separately.

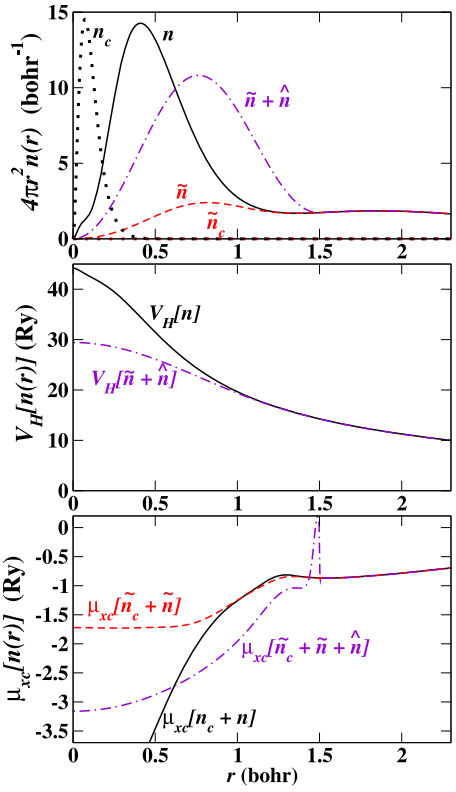

Fig. 5. Plots of radial charge densities (top panel), Hartree potentials (middle panel) and GGA exchange–correlation potentials (lower panel) for Si with $r_c^a = 1.5$ bohr. The compensation charge density $\hat{n}$ is constructed using the squared sinc function defined in Eq. (10).

all-electron valence Hartree potential as $r \to r_c^a$. The bottom panel of Fig. 4 shows the GGA exchange–correlation potential corresponding to the various charge densities. This plot shows that for the Blöchl formulation, $\mu_{xc}[\tilde{n}]$ smoothly converges to the all-electron exchange–correlation function $\mu_{xc}[n]$. On the other hand, for the Kresse formulation, $\mu_{xc}[\tilde{n}+\hat{n}]$ shows unphysical behavior near $r \leqslant r_c^a$ due to a significant discontinuity in the curvature of $[\tilde{n}+\hat{n}]$ in that region.

We also constructed a similar comparison of the densities and potentials for Si using the semicore configuration listed in Table 1 and the GGA exchange–correlation functional. The semicore configuration is necessary for accurately representing ionic materials such as SiO_2, but should also be able to accurately represent pure Si. The squared sinc function (10) was again used for the compensation charge shape. The results are shown in Fig. 5. In this case, there is a nontrivial core electron contribution $n_c(r)$, however because it is so localized within the augmentation radius, $\tilde{n}_c(r) \approx 0$. On the other hand, the compensation charge density $\hat{n}$ does contribute substantially to the pseudo exchange–correlation potential, and again causes a discontinuity in the vicinity of r_c^a.

An obvious question at this point is whether there might be a better choice of the compensation charge shape. In fact, the original paper describing their modified PAW formalism, Kresse et al. [14] introduced a shape based on a linear combination of Bessel functions similar to that used in RRKJ [19] pseudopotentials. A specific form can be written:

$$g_L^{\mathrm{B}}(r) = \begin{cases} \mathcal{N}_L[j_L(\frac{x_{L1}r}{r_{comp}}) - \frac{x_{L1}j_L'(x_{L1})}{x_{L2}j_L'(x_{L2})} j_L(\frac{x_{L2}r}{r_{comp}})] & \text{for } r \leqslant r_{comp}, \\ 0 & \text{for } r > r_{comp}, \end{cases} \quad (11)$$

where x_{Li} denotes the ith zero of the spherical Bessel function $j_L(x)$ and $\mathcal{N}_L$ denotes a normalization constant. As for the squared sinc function, this Bessel shape function is designed to vanish

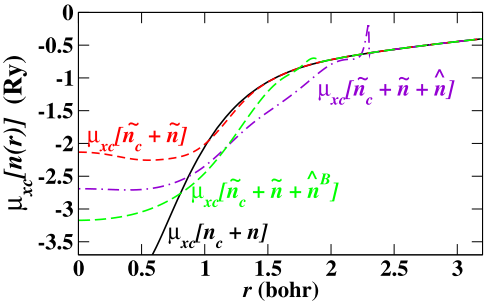

Fig. 6. GGA exchange–correlation potentials for Cu using $r_c^a = 2.3$ bohr, comparing functionals of all-electron density $(n_c + n)$, Blöchl's pseudodensity $(\tilde{n}_c + \tilde{n})$, and Kresse's pseudodensity $(\tilde{n}_c + \tilde{n} + \hat{n})$ using the squared sinc compensation charge shape, and $(\tilde{n}_c + \tilde{n} + \hat{n}^{\mathrm{B}})$ using the Bessel function compensation charge shape.

quadratically at the chosen radius. Kresse et al. recommend that the radius parameter be chosen such that $r_c^a/r_{comp} \approx 1.2$. Fig. 6 compares the GGA exchange–correlation functionals of Cu constructed using Blöchl's form and Kresse's form with two different compensation charge shapes both generated using the ATOMPAW code. In this example, we see that for using the Kresse form of the exchange–correlation treatment, the Bessel shape function for the compensation charge is numerically much better behaved than is the squared sinc function. However, it is again clear that the Blöchl form of the exchange–correlation treatment converges most smoothly to the all-electron function in the neighborhood of the augmentation sphere boundary.

These examples of discontinuous behavior of pseudo exchange–correlation potentials are obviously extreme cases, chosen to illustrate the problem clearly. In the examples shown in Figs. 4, 5, and 6 it is apparent that the discontinuities in the pseudo exchange–correlation potentials near r_c^a seem to be the likely cause of the discrepant structural results presented in Section 1. The pseudo exchange–correlation energy and potential contributions and related functions[2] within the augmentation sphere are designed to cancel out of the calculation. In practice, in each pair of canceling terms, one term is evaluated in Fourier space while the other is evaluated on a radial grid. The cancellation of these terms is only possible if their integrand functions are numerically well-behaved. Furthermore, the one-center terms defined in Eq. (1) are evaluated on radial grids centered on each atom. Their accurate evaluation relies on the assumption that the difference between the all-electron and pseudopotential contributions smoothly vanish in the vicinity of r_c^a, which is violated for the exchange–correlation contributions in these examples.

In order to verify our analysis of this problem we have written modified versions of the ATOMPAW, ABINIT, and PWPAW codes, allowing for the treatment of both the Blöchl and Kresse formulations of exchange–correlation energies (Eqs. (2) and (3)) and the corresponding Hamiltonian terms within each of the codes. Fig. 7 shows the results for Cu using the exchange–correlation functional, comparing both the Blöchl and Kresse forms using both of the modified codes. Here we see that all results using the Blöchl formalism are in excellent numerical agreement. The results from the two codes using the Kresse form with the squared sinc function have a relatively small numerical discrepancy with each other, undoubtedly due to slightly different treatments of the discontinuous exchange–correlation functional. The ABINIT code is also able to use the Bessel shape compensation charge (Eq. (11)) and those results are also shown in Fig. 7. In this case, both the Kresse and

[2] Because they are constructed by unscreening smooth local pseudopotentials, the local ionic potentials $(v_H^a[\tilde{n}_{Zc}])(r)$ defined in Ref. [14] or $\bar{v}^a(r)$ defined in Ref. [5]) are also affected by discontinuities in the pseudo exchange–correlation potential.

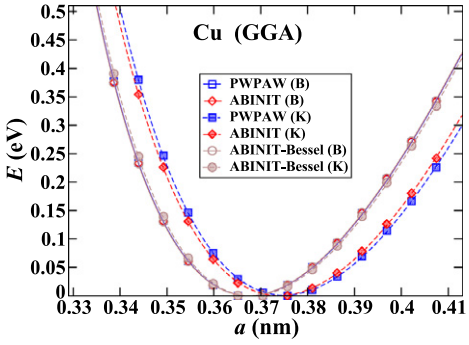

Fig. 7. Comparison of binding energy curves for Cu using the GGA exchange–correlation functional using the Blöchl (B) and Kresse (K) formalisms and the modified PWPAW and ABINIT codes. Also shown are results using the Bessel compensation charge shape (Eq. (11)) in both schemes using the ABINIT code.

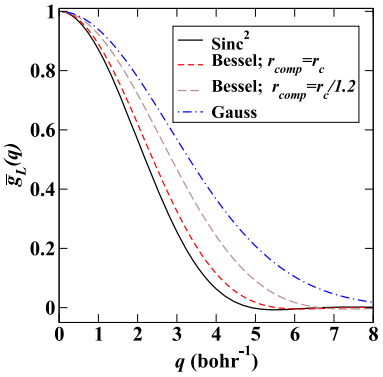

Fig. 8. Comparison of the Fourier transforms of various radial shape functions $g_L(r)$ for $L = 0$ using $r_c^a = 1.7$ bohr appropriate for Li PAW functions as described in Table 1.

Table 2
Ground state parameters for LiF, Si, and Cu determined from fit of calculations to the Murnaghan [20] equation of state, listing the equilibrium lattice constant a_0 (nm) and bulk modulus B (GPa). The notations (B) and (K) denote the Blöchl and Kresse formalisms for the exchange–correlation functionals respectively. For Si (v) and (s) denote the valence and semicore basis sets respectively detailed in Table 1. Most calculations used the squared sinc form (Eq. (10)) for the compensation charge shape; two calculations for Cu were performed using the Bessel function compensation charge shape (Eq. (11)) with the notation [Bes].

Method	LDA		GGA	
	a_0	B	a_0	B
	LiF			
WIEN2k	0.391	87	0.407	66
PWPAW (B)	0.392	85	0.408	66
ABINIT (K)	0.392	85	0.414	66
	Si			
WIEN2k			0.547	87
PWPAW (B) (v)			0.547	89
ABINIT (K) (v)			0.547	88
PWPAW (B) (s)			0.547	88
ABINIT (K) (s)			0.549	87
	Cu			
WIEN2k	0.355	170	0.366	130
PWPAW (B)	0.356	160	0.367	120
ABINIT (B)	0.356	160	0.367	120
ABINIT (B) [Bes]			0.367	120
ABINIT (K) [Bes]			0.368	120
PWPAW (K)			0.375	110
ABINIT (K)	0.357	160	0.374	110

Blöchl forms are in good agreement with each other and with the results of the Blöchl form using the squared sinc function.

Table 2 summaries the numerical results of all of the test cases considered in this work. The equilibrium lattice constants (a_0) and bulk moduli (B) were obtained by fitting the binding energy results to the Murnaghan equation of state [20].

4. Summary and conclusions

In this work, we have demonstrated that the original Blöchl PAW formalism for the exchange–correlation contributions (2) avoids numerical difficulties that can occur with the Kresse formulation (3). In order to clarify the issue, we have chosen extreme examples of the problem. From these examples, it is apparent that the origin of the problem is due to the fact that the exchange–correlation functions are very sensitive to the local shape of the density. Since these functionals were designed [8,9] to represent physical densities it is perhaps not surprising that the arbitrary shape of the valence compensation charge can cause spurious exchange–correlation contributions particularly when it is significantly larger than the physical density. We expect that this problem will become even more serious as more complicated functionals, which can depend on higher order density derivatives are developed [21].

In practice, the error we have identified can be ameliorated by choosing other radial shape functions than the squared sinc function defined in Eq. (10). The example for Cu using the Bessel function shape compensation charge defined in Eq. (11) illustrates this effect quite well. Another example of a popular form for the compensation charge is the Gaussian shape function used by Blöchl [5], which our tests show can give good numerical results for both the Blöchl and Kresse formalisms. One might worry that using these more localized compensation charge shapes generally increases the number of plane waves needed to converge the calculations. Fig. 8 illustrates the plane wave convergence of the various compensation charge shapes for $L = 0$ using the Li parameters ($r_c^a = 1.7$ bohr). The squared sinc function and the Bessel shape function with $r_{comp}^a = r_c^a$ converges significantly faster than the truncated Bessel shape function and the Gaussian shape function. In practice, for the several tests that we have studied, the convergence of the shape function does not appear to control the overall convergence of the PAW calculations. Several codes [5,3] make use of a Ewald [22] summation to further improve the convergence of the compensation charge contributions.

As a result of this analysis, we conclude that the Blöchl formulation of the exchange–correlation terms of the PAW method provides the best numerical stability. In principle, using the compensation charge contributions only for the Coulombic contributions for which they were designed, allows for greater choice in the shape functions which can give both physical results and optimized plane wave convergence parameters. Furthermore, the numerical evaluation of the exchange–correlation terms can be done more efficiently in the Blöchl formulation compared to the Kresse formulation since the evaluation of $\hat{n}$ within the exchange–correlation calculations is relatively time-consuming. A new version of ABINIT has been prepared and will be available in production release 6.1 and higher which has the option of using the Blöchl exchange–correlation formulation.

While we have argued that the Kresse formulation of the exchange–correlation terms of the PAW method is poorly motivated and can lead to numerical difficulties, we would like to stress that the problems we have identified affect a relatively small number of calculations. With careful control of the parameters, both the Blöchl and Kresse formulations of the PAW method can produce results consistent with all-electron results. The experiences learned in this analysis reinforces the fact that the quantitative accuracy of PAW and other pseudopotential methods relies on careful scrutiny and testing of the pseudopotential parameters used in the calculations. The ABINIT website (http://www.abinit.org) gives the following excellent advice: “Pseudopotentials should always

be tested in well-known situations, before using them for predictions."

Acknowledgements

We would like to acknowledge Bernard Amadon for fruitful discussions. The portion of this work performed at Wake Forest University was supported by NSF grants NSF DMR-0405456, DMR-0427055, and DMR-0705239 with computations performed on the Wake Forest University DEAC cluster, a centrally managed resource with support provided in part by the University. David Harris contributed to the database of PAW projector and basis functions available on the website http://www.wfu.edu/~natalie/papers/pwpaw/periodictable/periodictable.html over several summers while enrolled as a physics student at the University of North Carolina at Chapel Hill. WFU graduate students Nicholas Lepley and Xiao Xu also contributed to the database. Earlier work by summer students John Tumbleston and Nicholas Dellaripa is also acknowledged.

References

[1] P. Blaha, K. Schwarz, G. Madsen, D. Kvasnicka, J. Luitz, WIEN2k, An Augmented Plane Wave + Local Orbitals Program for Calculating Crystal Properties, Karlheinz Schwarz, Techn. Universität Wien, Austria, ISBN 3-9501031-1-2, 2001, http://www.wien2k.at.

[2] O.K. Andersen, Linear methods in band theory, Phys. Rev. B 12 (1975) 3060–3083.

[3] X. Gonze, B. Amadon, P.M. Anglade, J.M. Beuken, F. Bottin, P. Boulanger, F. Bruneval, D. Caliste, R. Caracas, M. Cote, T. Deutsch, L. Genovese, P. Ghosez, M. Giantomassi, S. Goedecker, D.R. Hamann, P. Hermet, F. Jollet, G. Jomard, S. Leroux, M. Mancini, S. Mazevet, M.J.T. Oliveira, G. Onida, Y. Pouillon, T. Rangel, G.M. Rignanese, D. Sangalli, R. Shaltaf, M. Torrent, M.J. Verstraete, G. Zerah, J.W. Zwanziger, Abinit: First-principles approach to material and nanosystem properties, Comput. Phys. Comm. 180 (2009) 2582–2615. Code is available at the website http://www.abinit.org.

[4] P. Giannozzi, S. Baroni, N. Bonini, M. Calandra, R. Car, C. Cavazzoni, D. Ceresoli, G.L. Chiarotti, M. Cococcioni, I. Dabo, A.D. Corso, S. de Gironcoli, S. Fabris, G. Fratesi, R. Gebauer, U. Gerstmann, C. Gougoussis, A. Kokalj, M. Lazzeri, L. Martin-Samos, N. Marzari, F. Mauri, R. Mazzarello, S. Paolini, A. Pasquarello, L. Paulatto, C. Sbraccia, S. Scandolo, G. Sclauzero, A.P. Seitsonen, A. Smogunov, P. Umari, R.M. Wentzcovitch, Quantum espresso: a modular and open-source software project for quantum simulations of materials, J. Phys.: Condens. Matter 21 (2009) 394402 (19 pp.). Available from the website http://www.quantum-espresso.org.

[5] P.E. Blöchl, Projector augmented-wave method, Phys. Rev. B 50 (1994) 17953–17979.

[6] P. Hohenberg, W. Kohn, Inhomogeneous electron gas, Phys. Rev. B 136 (1964) 864–871.

[7] W. Kohn, L.J. Sham, Self-consistent equations including exchange and correlation effects, Phys. Rev. A 140 (1965) 1133–1138.

[8] J.P. Perdew, Y. Wang, Accurate and simple analytic representation of the electron–gas correlation energy, Phys. Rev. B 45 (1992) 13244–13249.

[9] J.P. Perdew, K. Burke, M. Ernzerhof, Generalized gradient approximation made simple, Phys. Rev. Lett. 77 (1996) 3865–3868;
J.P. Perdew, K. Burke, M. Ernzerhof, Phys. Rev. Lett. 78 (1997) 1396 (Erratum).

[10] A.R. Tackett, N.A.W. Holzwarth, G.E. Matthews, A Projector Augmented Wave (PAW) code for electronic structure calculations, Part II: pwpaw for periodic solids in a plane wave basis, Comput. Phys. Comm. 135 (2001) 348–376. Available from the website http://pwpaw.wfu.edu.

[11] N.A.W. Holzwarth, A.R. Tackett, G.E. Matthews, A Projector Augmented Wave (PAW) code for electronic structure calculations, Part I: atompaw for generating atom-centered functions, Comput. Phys. Comm. 135 (2001) 329–347. Available from the website http://pwpaw.wfu.edu.

[12] N.A.W. Holzwarth, G.E. Matthews, A.R. Tackett, R.B. Dunning, Orthogonal polynomial projectors for the projector-augmented-wave (paw) method of electronic-structure calculations, Phys. Rev. B 57 (1998) 11827–11830.

[13] M. Valiev, J.H. Weare, The projector-augmented plane wave method applied to molecular bonding, J. Phys. Chem. A 103 (1999) 10588–10601.

[14] G. Kresse, D. Joubert, From ultrasoft pseudopotentials to the projector augmented-wave method, Phys. Rev. B 59 (1999) 1758–1775.

[15] P.E. Blöchl, C.J. Först, J. Schimpl, Projector augmented wave method: ab initio molecular dynamics with full wave functions, Bull. Mater. Sci. 26 (2003) 33–41.

[16] J.J. Mortensen, L.B. Hansen, K.W. Jacobsen, Real-space grid implementation of the projector augmented wave method, Phys. Rev. B 71 (2005) 035109 (11 pp.).

[17] M. Torrent, F. Jollet, F. Bottin, G. Zérah, X. Gonze, Implementation of the projector augmented-wave method in the abinit code: Application to the study of iron under pressure, Comput. Mater. Sci. 42 (2008) 337–351.

[18] S.G. Louie, S. Froyen, M.L. Cohen, Nonlinear ionic pseudopotentials in spin-density-functional calculations, Phys. Rev. B 26 (1982) 1738–1742.

[19] A.M. Rappe, K.M. Rabe, E. Kaxiras, J.D. Joannopoulos, Optimized pseudopotentials, Phys. Rev. B 41 (1990) 1227–1230;
A.M. Rappe, K.M. Rabe, E. Kaxiras, J.D. Joannopoulos, Phys. Rev. B 44 (1991) 13175–13176 (Erratum).

[20] F.D. Murnaghan, The compressibility of media under extreme pressures, Proc. Natl. Acad. Sci. USA 30 (1944) 244–247.

[21] J.P. Perdew, A. Ruzsinszky, G.I. Csonka, L.A. Constantin, J. Sun, Workhorse semilocal density functional for condensed matter physics and quantum chemistry, Phys. Rev. Lett. 103 (2009) 026403 (4 pp.).

[22] P.P. Ewald, Evaluation of optical and electrostatic lattice potentials, Ann. Phys. (Leipzig) 64 (1921) 253–287.